Science Advances

AAAS

Supplementary Materials for

Atomic-scale compositional mapping reveals Mg-rich amorphous calcium phosphate in human dental enamel

Alexandre La Fontaine, Alexander Zavgorodniy, Howgwei Liu, Rongkun Zheng, Michael Swain, Julie Cairney

The PDF file includes:

- fig. S1. Typical APT mass spectrum of human dental enamel containing organic materials (sample 1, Fig. 2).
- fig. S2. Mass spectra from different regions of human tooth enamel.
- fig. S3. Mass spectrum from N-rich region (organic).
- fig. S4. APT 3D reconstructed volumes of sample 3.
- fig. S5. APT 3D reconstructed volumes of samples 4 and 5.
- fig. S6. APT 3D reconstructed volumes of sample 6.
- table S1. Theoretical isotope proportion for Mg, C, and C_2 at 12, 12.5, and 13 daltons.
- table S2. Measured isotopic proportions at 12, 12.5, and 13 daltons in C-rich regions of enamel.
- table S3. Measured isotopic proportions at 12, 12.5, and 13 daltons in precipitate B.
- table S4. Measured isotopic proportions at 12, 12.5, and 13 daltons in intergranular ACP.
- table S5. Measured isotopic proportions at 12, 12.5, and 13 daltons in Mg-rich precipitate of sample 4.
- table S6. Typical composition of ACP, HAP, and Mg-rich precipitates in human dental enamel measured by APT.

Other Supplementary Material for this manuscript includes the following:
(available at advances.sciencemag.org/cgi/content/full/2/9/e1601145/DC1)

- movie S1 (.mp4 format). Animation showing the 3D distribution of Mg and Na atoms in human dental enamel; APT sample 3.
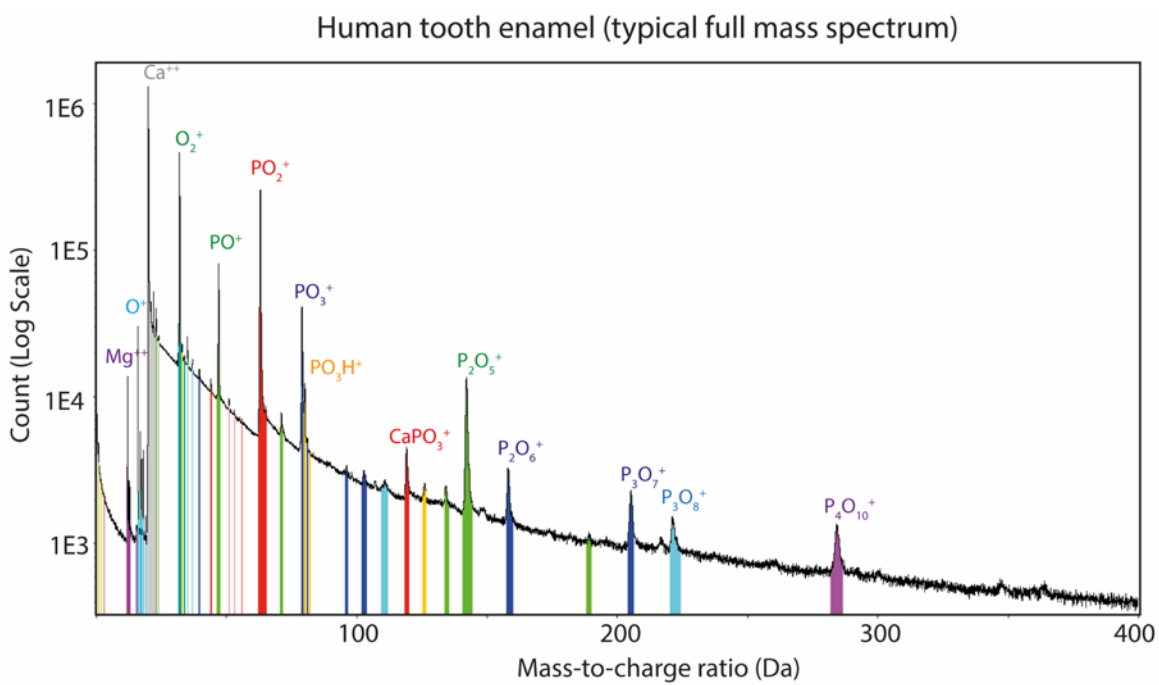
Supplementary Materials

fig. S1. Typical APT mass spectrum of human dental enamel containing organic materials (sample 1, Fig. 2).
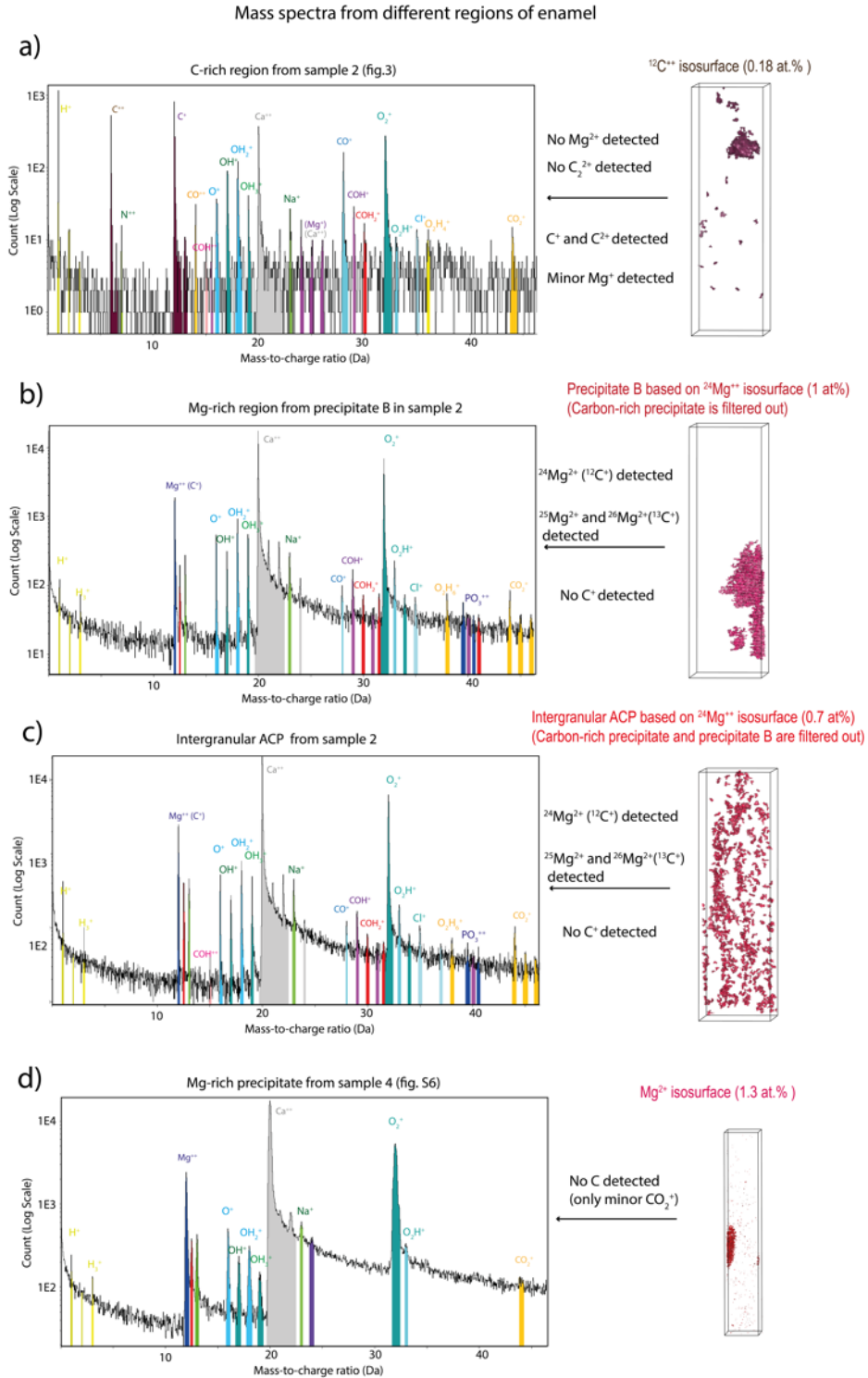
fig. S2. Mass spectra from different regions of human tooth enamel. (**a**) C-rich region from sample 2 (Fig. 3) based on 0.18 at.% $^{12}C^{2+}$ isosurface. (**b**) Mg-rich region from precipitate B, sample 2 (Fig. 3) based on 0.18 at.% $^{24}Mg^{2+}$ isosurface. (**c**) Intergranular Mg-ACP from sample 2 (Fig. 3) based on 0.7 at.% $^{24}Mg^{2+}$ isosurface. (**d**) Mg-rich precipitate from sample 4 (fig. S5) based on 1.3 at.% $^{24}Mg^{2+}$ isosurface.

Discussion on differentiating Mg from C in the human tooth enamel mass spectra

There is direct overlap between specific Mg and C ions in an atom probe mass-to-charge spectrum at 12, 12.5 and 13 Da, meaning that careful analysis is required to differentiate between Mg and C in the enamel mass spectra.

In this study, Mg is predominantly detected as Mg^{2+} (12, 12.5 and 13 Da). The Mg^+ peaks (24, 25, 26 Da) are minimal (only detected in one mass spectrum just above noise level; see S2-a); If there is any Mg^+ evaporating, it is too small to be detected above the thermal tail of $^{24}Ca^{2+}$; the most abundant Mg isotope, $^{24}Mg^+$, also overlaps with $^{48}Ca^{2+}$ (and potentially $^{24}C^{2+}$).

There are different potential overlaps at 12, 12.5 and 13 Da between Mg, C and C_2, summarized in table S1.

table S1. Theoretical isotope proportion for Mg, C, and C_2 at 12, 12.5, and 13 daltons.

Mass-to-charge (Da)	Possible ions	Theoretical isotopic proportion (at. %)
12	$^{24}Mg^{2+}$	78.99
	$^{12}C^+$	98.89
	$^{24}C_2^{2+}$	97.79
12.5	$^{25}Mg^{2+}$	10
	$^{25}C_2^{2+}$	2.19
13	$^{26}Mg^{2+}$	11
	$^{13}C^+$	1.11
	$^{26}C_2^{2+}$	0.01

H-containing species such as $^{12}C^1H^+$, $^{24}C_2{}^1H^{2+}$ or $^{24}Mg^1H^{2+}$ are potentially able to contribute to the 13 Da peak. However, if this were the case, one would expect a series of ions corresponding to a parent ion and between zero and a maximum number of H atoms to be visible in the mass spectrum, i.e. $^{12}CH_{0-3}{}^+$, $^{24}C_2H_{0-4}{}^{2+}$ or $^{24}MgH_{0-3}{}^{2+}$. Across all the data collected, there is no evidence for such ions. Moreover, no such peaks were observed in the mass spectra from C-rich and N-rich regions (figs. S2 and S3), which have higher H contents. While a contribution from these species to the peak at 13 Da cannot be entirely ruled out, it is thought to be highly unlikely.

At 12 Da, there are 3 possible overlapping peaks: $^{24}Mg^{2+}$, $^{12}C^+$ and $^{24}C_2^{2+}$. These three isotopes are the most abundant of their series, at abundances of 78.99 at. %, 98.89 at. % and 97.79 at. %, respectively. At 12.5 Da, $^{25}Mg^{2+}$ overlaps with $^{25}C_2^{2+}$. However, only 2.19 at. % of the total C_2^{2+} would contribute to that peak as $^{25}C_2^{2+}$, which contrasts with 10 at. % of the total Mg^{2+} from $^{25}Mg^{2+}$. A similar situation occurs for the peak at 13 Da, with three potential overlaps between $^{26}Mg^{2+}$, $^{13}C^+$ and $^{26}C_2^{2+}$, although there is a substantial difference in the contributions to this peak, with $^{26}Mg^{2+}$ accounting for 11 at. % of Mg^{2+}, $^{13}C^+$ 1.11 at. % of total C^+ and $^{26}C_2^{2+}$ 0.01 at. % of total C_2^{2+}.

The overlap between these three species is direct. It is thus impossible to use deconvolution techniques to differentiate them. There are however different ways to distinguish between Mg and C:

- Extracting the mass spectrum from carbon-rich regions (using isosurfaces based on $^{12}C^{2+}$ at 6 Da) and investigating the presence and amount of C^{2+}, C_2^{2+}, and other carbon peaks.
- Extracting the mass spectrum from (supposed) Magnesium-rich regions (based on the absence of $^{12}C^{2+}$ at 6 Da) and comparing it with the carbon-rich region mass spectrum.
- Checking the deviation of the measured (supposed) Mg^{2+} peaks abundances with the theoretical values for Mg.

* Important note on the isotopic proportions measurement method:

Each peak was ranged from noise to noise. The standard deviations were calculated using the formula
$\sqrt{(Background + Uncorrected\ Signal)}$. *The local range-assisted background model was used in IVAS to perform the background correction.*

Note that the tail of the peak at 12 Da could contribute to the measured amount of the peak at 12.5 Da and both tails could also contribute to the 13 Da peak. This cannot be perfectly corrected and as a result the calculated standard deviations do not fully reflect the real uncertainties in the measured proportions.

<u>Carbon-rich regions do not contain C_2^{2+}</u>

In the mass spectrum from the carbon-rich region of sample 2 (fig. S2-a) C peaks are detected as $^{12}C^+$ / $^{24}C_2^{2+}$ (12 Da), $^{13}C^+$ (13 Da) and $^{12}C^{2+}$(6 Da), $^{13}C^{2+}$ (6.5 Da). However, there is no peak detected at 12.5 Da which rules out presence of significant quantities of $^{25}C_2^{2+}$.

Similarly, if significant Mg^{2+} was present, $^{25}Mg^{2+}$, accounting for 10 at. % of the whole Mg^{2+} should be detected at 12.5 Da. For example, the peak at 12 Da in fig. S2-a is around 1206 counts. The detection limit at 12.5 Da is estimated at around 10 counts. The maximum possible contribution of $^{24}Mg^{2+}$ at 12 Da would then be around 79 counts which represents 6.5 % of the total peak at 12 Da. To a lesser extent, the same is valid for $^{25}C_2^{2+}$ which accounts for 2.19 at. % of the whole C_2^{2+}.

Moreover, the measured isotopic proportion of $^{12}C^+$ and $^{13}C^+$ is quite close to the theoretical value as shown in table S2.

table S2. Measured isotopic proportions at 12, 12.5, and 13 daltons in C-rich regions of enamel.

	Mass-to-charge (Da)	Net counts	Measured isotopic proportion (at. %)
Carbon-rich region (sample 2)	12	1206 ± 35	97.9 ± 2.8
	12.5	not detected	n/a
	13	25 ± 6	2.1 ± 0.5

The combination of no peak detected at 12.5 Da, a measured isotopic ratio $^{12}C^+/^{13}C^+$ within experimental error of its theoretical value and the presence of $^{12}C^{2+}$ and $^{13}C^{2+}$ leads us to conclude that Mg^{2+} and C_2^{2+} are absent in the C-rich region mass spectrum.

While the absence of Mg^{2+} in the carbon-rich region mass spectrum allows for clear determination of the different carbon peaks, the most important finding is the absence of C_2^{2+}. Considering that all the data sets were collected using very similar experimental parameters, equivalent to similar field conditions, we can safely assume that C_2^{2+} is not present (at least not detectable) in any of the enamel mass spectra. This allows us to rule out any major overlap at 12.5 Da, so that only $^{25}Mg^{2+}$ contributes to this peak.

Magnesium and carbon-rich precipitate:

The precipitate B from sample 2 (fig. 3-5 and S2-b) also contains a significant amount of carbon (presence of $^{12}C^{2+}$ at 6 Da), together with, presumably, a large amount of Mg (presence of peaks at 12, 12.5, and 13). Based on the previous discussion, C_2^{2+} is ruled out leaving only $^{12}C^+$, $^{13}C^+$ and $^{24}Mg^{2+}$, with $^{26}Mg^{2+}$ being the principal contribution to the peaks at 12 and 13 Da. Table S3 shows the measured isotopic proportions of the three peaks.

table S3. Measured isotopic proportions at 12, 12.5, and 13 daltons in precipitate B.

	Mass-to-charge (Da)	Net counts	Measured isotopic proportion (at. %)
Precipitate B (sample 2)	12	6393 ± 83	78.1 ± 1
	12.5	773 ± 36	9.4 ± 0.4
	13	1017 ± 39	12.4 ± 0.5

These proportions are very close to the theoretical values for Mg^{2+}. Due to the presence of $^{12}C^{2+}$ one would expect some small contribution of $^{12}C^+$. In the mass spectrum from the carbon-rich region (fig. S2-a), $^{12}C^{2+}$ was around 1000 counts and $^{12}C^+$ around 1206 counts. By extrapolation, we could estimate the $^{12}C^+$ contribution around 1.2 times the $^{12}C^{2+}$ peak. With $^{12}C^{2+}$ at around 50, the contribution of $^{12}C^{2+}$ to the peak at 12 Da would be around 60 Da, which is about 1 % of the total peak. As mentioned earlier, there are many sources of uncertainties involved in such measurements such as tail contribution from the previous peak to the next one, the accuracy of background removal model as well as peak ranging. However, these results provide a high degree of confidence in our ability to differentiate between C and Mg.

Intergranular ACP phase:

The mass spectrum from the intergranular region in sample 2 (S2-c) does contain a large amount of Mg (based on the presence of peaks at 12, 12.5 and 13). $^{12}C^{2+}$ was not detected at 6 Da. However, carbon is present, detected as molecular ions.

The following table shows the isotopic proportions for Mg^{2+} at 12, 12.5 and 13 Da. (table S4) The measured proportion are again quite close to theoretical Mg^{2+} isotopic proportions although the $^{24}Mg^{2+}$ seems a bit smaller than usual. It is worth noting that this trend occurs in most of the intergranular ACP mass spectra. Despite this slight difference, these results are still very convincing, with Mg^{2+} contributing mostly to the three peaks.

table S4. Measured isotopic proportions at 12, 12.5, and 13 daltons in intergranular ACP.

	Mass-to-charge (Da)	Net counts	Measured isotopic proportion (at. %)
	12	7296 ± 90	76.1 ± 1
Precipitate sample 4	12.5	1120 ± 35	11.6 ± 0.4
	13a	1170 ± 36	12.2 ± 0.4

Magnesium-rich precipitate:

The precipitate from sample 4 (S6 and S2-d) does contain a large amount of Mg (presence of peaks at 12, 12.5 and 13). Carbon was only detected as CO^{2+}, and just above noise level. The following table shows the isotopic proportions for Mg2+ at 12, 12.5 and 13 Da (table S3). These results again confirm the principal contribution from Mg^{2+} to the three peaks.

table S5. Measured isotopic proportions at 12, 12.5, and 13 daltons in Mg-rich precipitate of sample 4.

	Mass-to-charge (Da)	Net counts	Measured isotopic proportion (at. %)
	12	10605 ± 100	77.9 ± 1
Precipitate sample 4	12.5	1344 ± 45	9.9 ± 0.4
	13	1652 ± 50	12.1 ± 0.5

Conclusions:

We were able to rule out the presence of C_2^{2+} in enamel mass spectrum. We also were able to demonstrate a good match between the theoretical and experimental isotopic proportions of Mg^{2+}. While we cannot rule out completely the contribution of any C to the Mg peaks, the evidence presented here leads us to conclude that it is minimal.
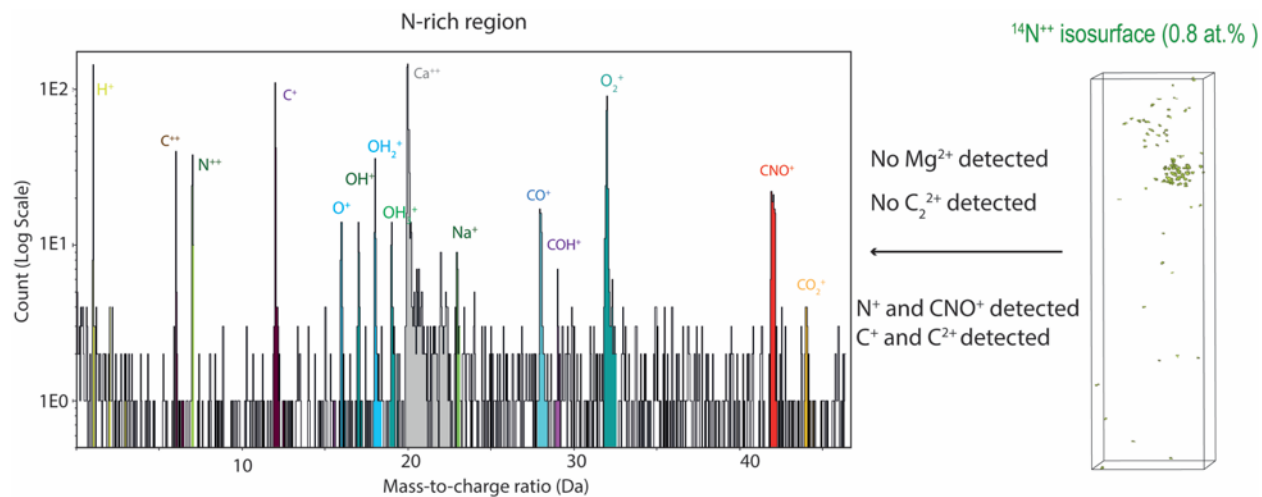
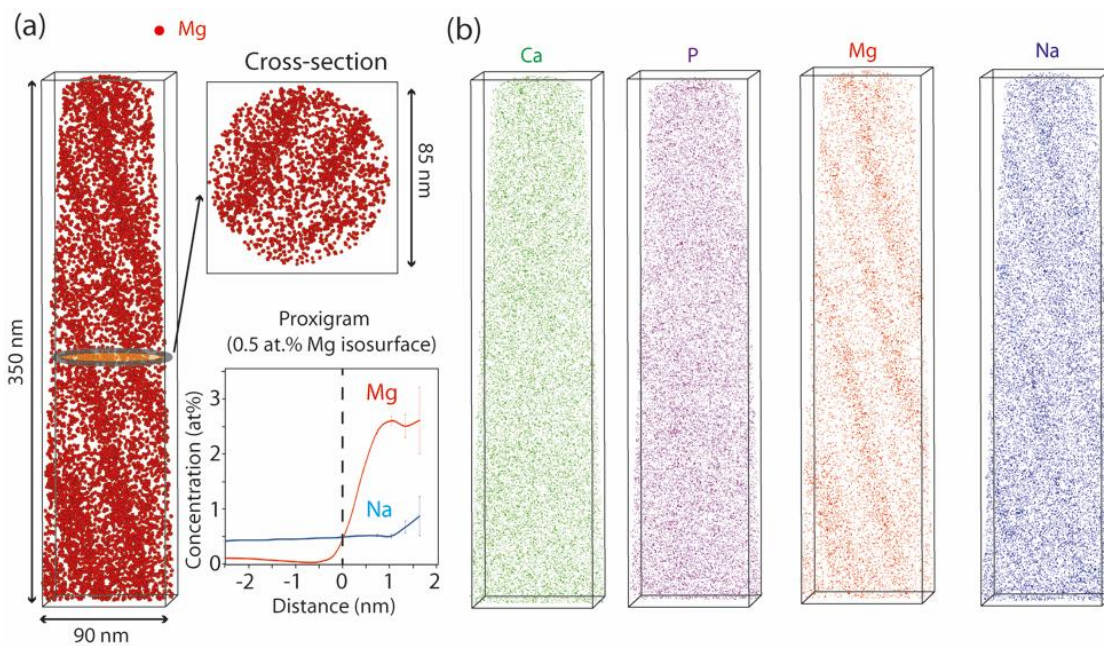**fig. S3. Mass spectrum from N-rich region (organic).**

fig. S4. APT 3D reconstructed volumes of sample 3. (**a**) Atom maps of Mg (8 nm slices) with two orientations (along the tip and cross-section). Proxigram analysis of Mg-ACP based on 0.5 at.% Mg isosurface. (**b**) atom maps of Ca, P, Mg and Na (8nm slices).
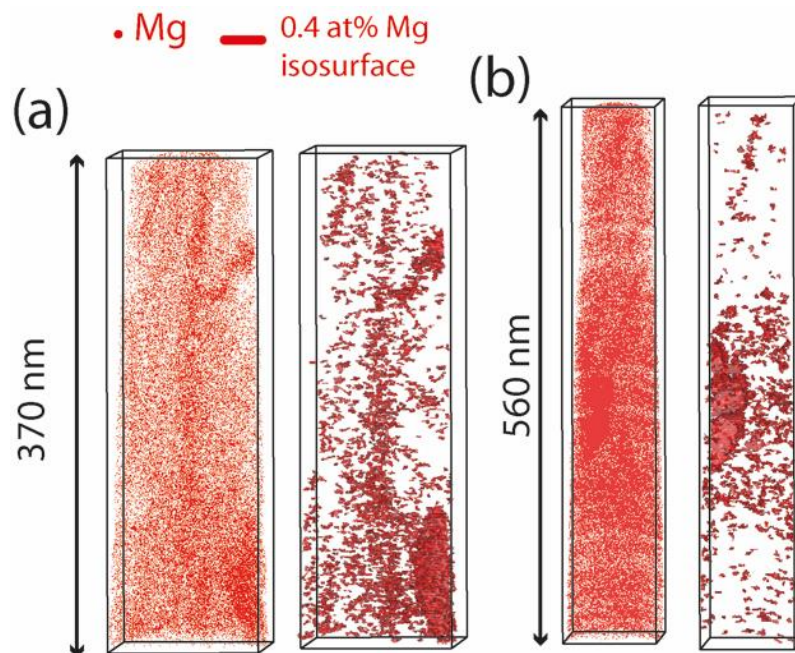
fig. S5. APT 3D reconstructed volumes of samples 4 and 5. Atom maps of Mg and 0.4 at.% Mg isosurface of (**a**) sample 4 and (**b**) sample 5. Note the two elongated Mg-rich precipitates.
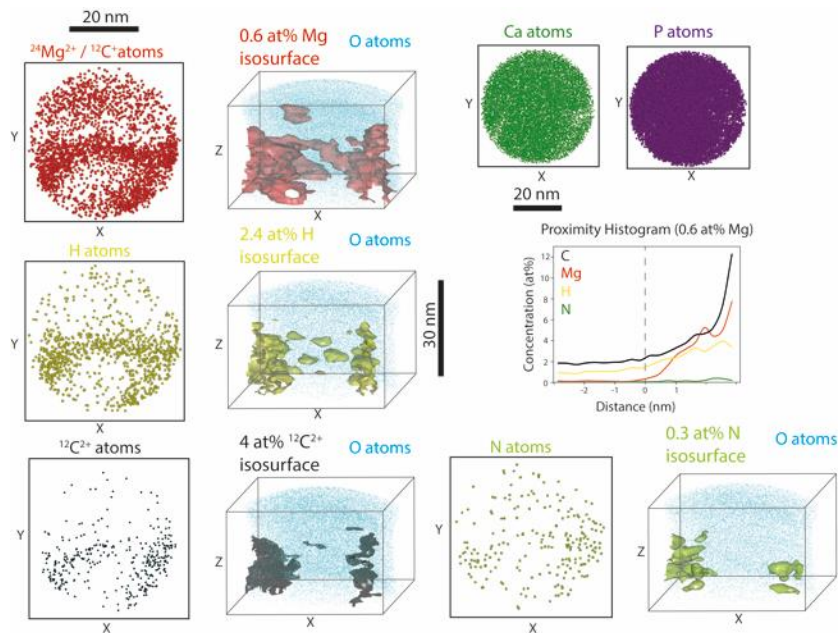

fig. S6. APT 3D reconstructed volumes of sample 6. Atom maps of Mg, H, C and N. Volumes with isosurfaces of

Mg (0.6 at.%), H (2.4 at.%), C (4 at.%) and N (0.3 at.%) and O atoms. Note the organic materials remnants (C, H,

N). This APT data-set is limited in size due to the rapid fracture of the tip.

table S6. Typical composition of ACP, HAP, and Mg-rich precipitates in human dental enamel measured by APT.

Element (wt%)	Sample 1 (fig. 2)		Sample 2 (fig. 3)			
	Mg-rich ACP	HAP crystallites	Mg-rich ACP	HAP crystallites	Precipitate A	Precipitate B
Ca	38.5 ± 0.1	37.1 ± 0.02	37.1 ± 0.1	35.3 ± 0.02	18.9 ± 0.1	31.3 ± 0.1
P	21.8 ± 0.1	23.4 ± 0.02	21.7 ± 0.1	23.9 ± 0.02	16.4 ± 0.1	24.7 ± 0.1
O	37.0 ± 0.1	38.6 ± 0.02	37.3 ± 0.2	39.8 ± 0.04	46.1 ± 0.2	40.7 ± 0.2
Mg	1.55 ± 0.02	0.15 ± 0.002	2.66 ± 0.02	0.11 ± 0.002	0.10 ± 0.05	2.24 ± 0.02
Na	0.51 ± 0.02	0.26 ± 0.002	0.35 ± 0.02	0.24 ± 0.002	0.51 ± 0.02	0.33 ± 0.01
C	0.22 ± 0.02	0.14 ± 0.004	0.42 ± 0.005	0.23 ± 0.004	15.60 ± 0.02	0.39 ± 0.01
N	not detected	not detected	not detected	not detected	0.16 ± 0.02	not detected
H	0.13 ± 0.02	0.10 ± 0.01	0.14 ± 0.02	0.10 ± 0.02	1.00 ± 0.02	0.13 ± 0.01
Cl	0.25 ± 0.02	0.32 ± 0.002	0.29 ± 0.02	0.34 ± 0.002	1.31 ± 0.02	0.15 ± 0.02
Ca/P ratio	1.76	1.59	1.70	1.48	1.15	1.26

movie S1. Animation showing the 3D distribution of Mg and Na atoms in human dental enamel; APT sample 3.